

# Real-time gravitational-wave inference for binary neutron stars using machine learning

Maximilian Dax,<sup>1,\*</sup> Stephen R. Green,<sup>2,†</sup> Jonathan Gair,<sup>3</sup> Nihar Gupte,<sup>3,4</sup> Michael Pürrer,<sup>5,6</sup> Vivien Raymond,<sup>7</sup> Jonas Wildberger,<sup>1,8</sup> Jakob H. Macke,<sup>1,9</sup> Alessandra Buonanno,<sup>3,4</sup> and Bernhard Schölkopf<sup>1,8</sup>

<sup>1</sup>*Max Planck Institute for Intelligent Systems, Max-Planck-Ring 4, 72076 Tübingen, Germany*

<sup>2</sup>*School of Mathematical Sciences, University of Nottingham,  
University Park, Nottingham NG7 2RD, United Kingdom*

<sup>3</sup>*Max Planck Institute for Gravitational Physics (Albert Einstein Institute), Am Mühlenberg 1, 14476 Potsdam, Germany*

<sup>4</sup>*Department of Physics, University of Maryland, College Park, MD 20742, USA*

<sup>5</sup>*Department of Physics, East Hall, University of Rhode Island, Kingston, RI 02881, USA*

<sup>6</sup>*Center for Computational Research, Carothers Library,  
University of Rhode Island, Kingston, RI 02881, USA*

<sup>7</sup>*Gravity Exploration Institute, Cardiff University, Cardiff CF24 3AA, United Kingdom*

<sup>8</sup>*ELLIS Institute Tübingen, Maria-von-Linden-Straße 2, 72076 Tübingen, Germany*

<sup>9</sup>*Machine Learning in Science, University of Tübingen & Tübingen AI Center, 72076 Tübingen, Germany*

Mergers of binary neutron stars (BNSs) emit signals in both the gravitational-wave (GW) and electromagnetic (EM) spectra. Famously, the 2017 multi-messenger observation of GW170817 [1, 2] led to scientific discoveries across cosmology [3], nuclear physics [4–6], and gravity [7]. Central to these results were the sky localization and distance obtained from GW data, which, in the case of GW170817, helped to identify the associated EM transient, AT 2017gfo [8], 11 hours after the GW signal. Fast analysis of GW data is critical for directing time-sensitive EM observations; however, due to challenges arising from the length and complexity of signals, it is often necessary to make approximations that sacrifice accuracy. Here, we develop a machine learning approach that performs complete BNS inference in just one second without making any such approximations. This is enabled by a new method for explicit integration of physical domain knowledge into neural networks. Our approach enhances multi-messenger observations by providing (i) accurate localization even before the merger; (ii) improved localization precision by  $\sim 30\%$  compared to approximate low-latency methods; and (iii) detailed information on luminosity distance, inclination, and masses, which can be used to prioritize expensive telescope time. Additionally, the flexibility and reduced cost of our method open new opportunities for equation-of-state and waveform systematics studies. Finally, we demonstrate that our method scales to extremely long signals, up to an hour in length, thus serving as a blueprint for data analysis for next-generation ground- and space-based detectors.

**Introduction.**—Fast and accurate inference of binary neutron stars (BNSs) from gravitational-wave (GW) data is a critical challenge facing multi-messenger astronomy. Indeed, for a BNS, the GW signal is visible by the LIGO-Virgo-KAGRA (LVK) [9–11] observatories minutes before any electromagnetic counterpart. The signal encodes advance information on source characterization, distance, sky location, and orientation necessary for prioritizing and pointing optical telescopes. However, the length of BNS signals makes conventional Bayesian inference techniques [12, 13] too slow to be useful in low-latency applications. Instead, once a signal is identified by detection pipelines [14–21], approximate algorithms are used for providing initial alerts (e.g., Bayestar [22], which uses the signal-to-noise [SNR] time series rather than the complete strain data and gives localization in seconds). Other methods focus on accelerating likelihood evaluations without incurring loss of precision (e.g., using reduced-order quadratures), with the state-of-the-art delivering localization in six minutes, and full inference in two hours [23].

In this study, we develop a machine-learning method

that can perform full BNS inference in just one second, providing estimates of all 17 parameters without making any (practically relevant) approximations and with strong accuracy guarantees. Building on the DINGO framework [24–27], we train a neural network with millions of simulations to encode theoretical GW models. We present several innovations that enable us to scale such neural networks to BNS signals with durations up to a thousand times longer than the binary black holes we analyzed previously at high accuracy with machine learning. Once trained, the network takes measured GW data as input and computes probabilistic estimates of the corresponding BNS source parameters (Fig 1). Our algorithm, called DINGO-BNS, can also infer all of these parameters *minutes before the merger* based on partial inspiral-only information, estimates which can be continuously updated as more data become available (Fig. 2a). Near-real-time or pre-merger alerts can then be provided to astronomers, facilitating potential discoveries of precursor and prompt electromagnetic counterparts [28–30]. The approach also affords a great deal of flexibility, enabling new prospects for interaction with multi-messenger observers and efficient offline analyses.

Since DINGO-BNS performs (asymptotically) exact inference from GW strain data, it provides substantially im-

\* maximilian.dax@tuebingen.mpg.de

† stephen.green2@nottingham.ac.uk

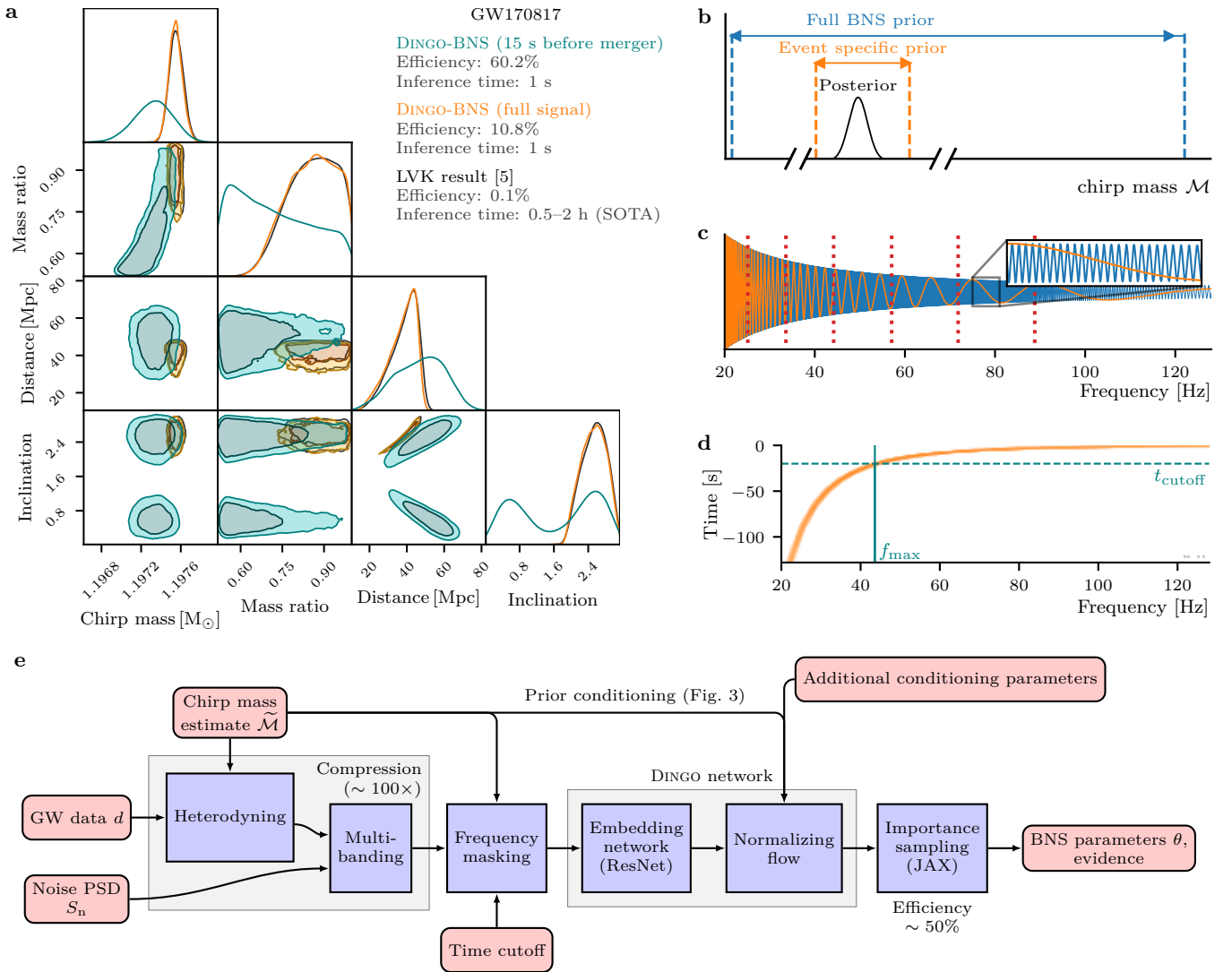


Figure 1. **Real-time GW inference for BNS is enabled by several innovations.** (a) DINGO-BNS estimates all BNS parameters in just one second (orange), reproducing LVK results [5] (black) three orders of magnitude faster than existing methods [23, 31]. DINGO-BNS can also analyze partial data before the merger occurs (teal). These speed improvements are largely due to precise neural network inference, leading to high importance sampling efficiency (indicated in the legend). Fast analysis results are crucial for directing electromagnetic searches for prompt or even precursor signals. (b) For a given event, the chirp mass posterior (black) is tightly constrained compared to the prior (blue), so a restricted chirp mass prior (orange) is sufficient, and moreover simplifies analysis. With our novel prior-conditioning technique, we train a single neural network that can be instantly tuned to an event-specific prior lying anywhere within the full volume. (c) We compress data by a factor of  $\sim 100$  by first factoring out (“heterodyning”) the predominant phase evolution of the signal (blue), based on a chirp mass estimate  $\tilde{\mathcal{M}}$  associated to the event-specific prior. The resulting simplified signal (orange) is down-sampled in resolution, reducing data dimensionality (coarser resolution at high frequencies; bands indicated by dotted red lines). (d) To enable pre-merger inference, we mask out the strain frequency series according to the cut-off time. (e) All of these components are integrated into a single neural network that can be trained end-to-end and produce  $10^5$  weighted samples per second, with typical sampling efficiencies of 50%.

proved precision in comparison to low-latency algorithms that make additional approximations. Indeed, for sky localization, we achieve median reductions in the size of the 90% credible region of around 30% compared to Bayestar across a range of simulated data sets (Fig. 2b). This corresponds to a reduction in required optical telescope

time, increasing the likelihood of finding a counterpart and observing it in its earliest stages. For next-generation detectors (XG, e.g., Cosmic Explorer [32] and Einstein Telescope [33]), signals will be longer so pre-merger inference will become even more important [34]. We have tested DINGO-BNS in an XG setting, and shown that

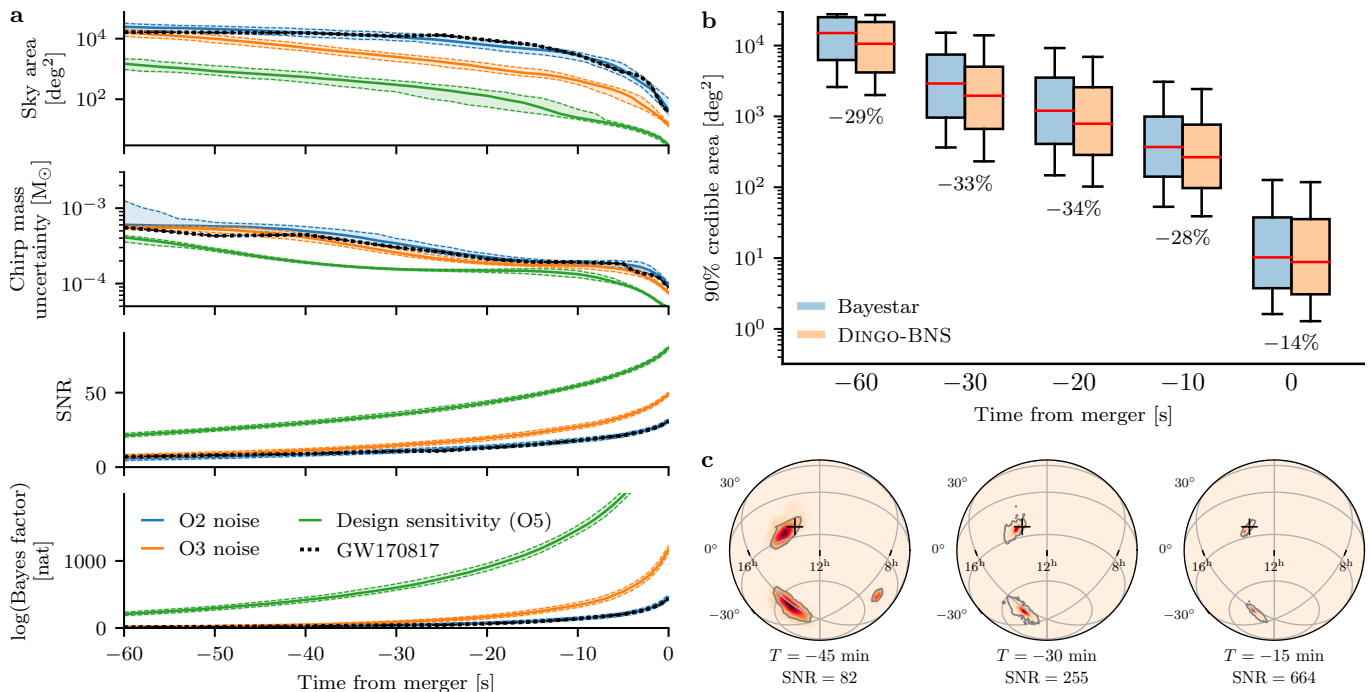


Figure 2. **Pre-merger inference with DINGO-BNS.** (a) Evolution of pre-merger estimates for GW170817 (black) and GW170817-like simulations injected into different noise levels (colors). We display the 90% credible sky area, the standard deviation of the chirp mass, the accumulated signal-to-noise and the log Bayes factor comparing the signal and noise models. All of these quantities are inferred with a latency of  $\sim 1$  second. (b) Sky localization area at 90% credible level for various premerger times, comparing against Bayestar. The boxplots display the median (red line), quartiles (colored box) and 10th/90th percentiles (whiskers). DINGO-BNS localization is consistently more precise. (c) Premerger sky localization for a GW170817-like event injected into Cosmic Explorer noise, using a minimum frequency of 6 Hz. The black marker indicates the injection coordinates, and gray outline the 90% credible area.

our optimizations enable rapid pre-merger inference for signals up to an hour in length (Fig. 2c). These signals would be impossible to treat in low latency using conventional methods. DINGO-BNS, moreover, estimates *all* BNS parameters (including constituent masses, tidal deformabilities, luminosity distance, and inclination angle) which will be crucial for prioritizing the use of expensive telescope time for the most interesting targets as event rates continue to increase.

**Related work.**—Machine learning for GW astronomy is an active area of research [35]. Several studies explore machine learning inference for black hole mergers [24–27, 36–43]. There have also been applications specifically to BNS inference, notably the GW-SkyLocator algorithm [44], which estimates the sky position using the SNR time series (similar to Bayestar), and JIM [31, 45], which uses hardware acceleration and machine learning to speed up conventional samplers and achieve full inference in 25 minutes. The ASTREOS framework uses machine learning for BNS equation-of-state inference [46]. Pre-merger localization with conventional techniques has also been explored in [47].

**DINGO-BNS.**—Our framework uses neural simulation-based inference (SBI) to estimate an

amortized posterior [48]. For given GW data  $d$ , the source is characterized in terms of the posterior probability distribution  $p(\theta|d)$  over BNS parameters  $\theta$ . For a BNS, there are 17 parameters: the component masses (2), spins (6), orientation, sky position (2), luminosity distance, polarization, time and phase of coalescence, and (in contrast to black holes) tidal deformabilities (2). Following [26], we use simulated GW datasets to train a density estimation neural network  $q(\theta|d)$  (a normalizing flow) to approximate  $p(\theta|d)$ . Once trained, inference for any new data  $d$  simply requires sampling  $\theta \sim q(\theta|d)$ —thus amortizing training costs across all observations. We obtain asymptotically exact results by augmenting the neural network samples with importance weights using the GW likelihood function [49]. This framework, called DINGO-IS [27], has been successfully applied to black hole mergers (see Supplemental Material). BNS signals, however, are much longer than those of binary black holes, up to hundreds of seconds for LVK-like detectors (compared to roughly ten for binary black holes) and potentially hours for XG, rendering the naïve transfer of existing machine learning methods to BNS signals impossible.

DINGO-BNS addresses this challenge using several

*event-tuned* design choices (Fig. 1e). These include using knowledge of specific BNS signal morphology to drastically compress the data sets in a non-lossy way; conditioning the network on the compressor using a new technique called prior-conditioning; frequency masking based on the pre-merger time and chirp mass; and conditioning on parameter subsets for incorporating multi-messenger information or expectations from nuclear models. The philosophy underlying our approach is that the full BNS problem is too hard for existing neural architectures, so we divide the parameter and data spaces into manageable portions based on known physical information. We then combine all of these variable design choices into a single network that we can instantly tune to the context at hand.

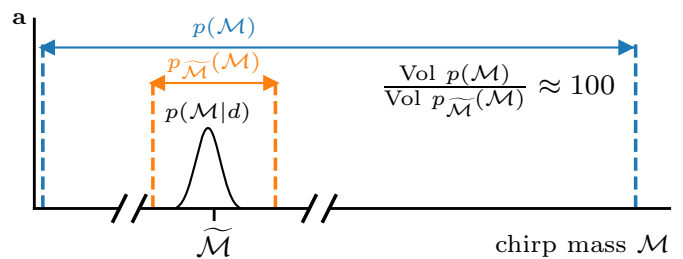
**Data compression and prior conditioning.**—Our data compression adapts two GW analysis techniques to the SBI context, heterodyning [50, 51] (also known as relative binning [52]) to simplify the data, and multibanding [53, 54] to reduce the data dimension without loss of information. During the long inspiral period, a BNS signal exhibits a “chirp,” with phase evolution to leading order in the post-Newtonian expansion [55] given by

$$\varphi(f; \mathcal{M}) = \frac{3}{128} \left( \frac{\pi G \mathcal{M} f}{c^2} \right)^{-5/3}, \quad (1)$$

where  $\mathcal{M} = (m_1 m_2)^{3/5} / (m_1 + m_2)^{1/5}$  is the chirp mass of the system, with  $m_1, m_2$  the component masses. Given an approximation  $\tilde{\mathcal{M}}$  to the chirp mass, we heterodyne the (frequency-domain) data by multiplying by  $e^{i\varphi(f; \tilde{\mathcal{M}})}$ , reducing the number of oscillations in the signal by several orders of magnitude (Fig. 1c). Given heterodyned data, we apply multibanding by partitioning the domain into (empirically-determined) frequency bands, and coarsening the resolution in higher bands such that the (heterodyned) signal is preserved.

Our compression, however, cannot be done across the entire BNS prior volume using a single value of  $\tilde{\mathcal{M}}$ . DINGO-BNS therefore uses a new method that we call “prior-conditioning,” whereby we restrict to an event-specific prior over which we compress the data, but train a network that is *tunable* to this choice of restriction (Fig. 3). Inference requires an estimate  $\tilde{\mathcal{M}}$  of the chirp mass  $\mathcal{M}$ , which can be determined quickly by sweeping across the prior (see Supplemental Material).

**Frequency masking.**—In contrast to past work, DINGO-BNS also allows for strain frequency series with varying  $f_{\min}$  and  $f_{\max}$ . For a given analysis,  $f_{\min}$  is chosen based on  $\mathcal{M}$  and the segment duration, as the minimum frequency present in the signal in a given GW detector network. This masking is necessary for consistency with frequency-domain waveform models, which assume infinite duration. Choosing  $f_{\max}$ , by contrast, determines the end time of the data stream analyzed to enable pre-merger inference (see Supplemental Material).



**b Training step**

- 1:  $\tilde{\mathcal{M}} \sim \hat{p}(\tilde{\mathcal{M}})$  ▷ Sample  $\tilde{\mathcal{M}}$  from hyperprior
- 2:  $\mathcal{M} \sim p_{\tilde{\mathcal{M}}}(\mathcal{M})$  ▷ Sample  $\mathcal{M}$  from restricted prior
- 3:  $d \leftarrow d(\mathcal{M})$  ▷ Simulate data
- 4:  $d_{\tilde{\mathcal{M}}} \xleftarrow{\tilde{\mathcal{M}}} d$  ▷ Compress data, see (1c)
- 5: Optimize  $-\log q(\mathcal{M} - \tilde{\mathcal{M}} | d_{\tilde{\mathcal{M}}}, \tilde{\mathcal{M}})$

**c Inference**

- Require:  $\tilde{\mathcal{M}} \approx \mathcal{M}_{\text{true}}$  ▷ Choose approximate  $\tilde{\mathcal{M}}$
- 1:  $d_{\tilde{\mathcal{M}}} \xleftarrow{\tilde{\mathcal{M}}} d$  ▷ Compress data
  - 2:  $\delta\mathcal{M} \sim q(\delta\mathcal{M} | d_{\tilde{\mathcal{M}}}, \tilde{\mathcal{M}})$  ▷ Sample  $\delta\mathcal{M}$  from network
  - 3:  $\mathcal{M} \leftarrow \tilde{\mathcal{M}} + \delta\mathcal{M}$

Figure 3. **Prior conditioning enables event-specific compression.** We train an SBI model simultaneously across a range of priors, each parametrized by a reference chirp mass  $\tilde{\mathcal{M}}$ . For each (narrow) prior  $p_{\tilde{\mathcal{M}}}(\mathcal{M})$ , we apply the compression (heterodyning and multibanding). This compression simplifies the data distribution that the model must learn and reduces its dimensionality. For simplicity in this presentation, we omit parameters other than the chirp mass.

**Conditioning on parameter subsets.**—The DINGO-BNS framework (and SBI in general) allows for a great deal of flexibility in terms of quickly marginalizing over and conditioning on parameters. Conditioning on a parameter allows us to set it to a fixed value, e.g., to incorporate knowledge of that parameter from other sources. To train a conditional network, we provide it as additional input and exclude it from the set of parameters to infer.

In our study, we trained DINGO-BNS networks conditioned on the sky position, i.e., we learned the distribution  $p(\theta \setminus \{\alpha, \delta\} | d, \alpha, \delta)$ , where  $\alpha, \delta$  denote the right ascension and declination, respectively. This allows us to incorporate precise multi-messenger localization to obtain tighter constraints on the remaining parameters. In the context of multi-messenger astronomy, such networks could be used to provide real-time feedback on whether candidates observed by optical telescopes within large GW sky regions should be prioritized for detailed spectroscopy [56]. This way, DINGO-BNS can enable new modes of interaction between GW and electromagnetic observers, potentially transforming how we prioritize and respond to multi-messenger events.

Parameter-conditioning can also accelerate offline analyses of the nuclear equation-of-state. With a DINGO-BNS network conditioned on component masses and

tidal deformabilities, we can rapidly compute conditional Bayesian evidences which allows for comparatively cheap computation of equation-of-state likelihoods (see Supplemental Material).

**Experiments.**—We generate training data using the IMRPhenomPv2\_NRTidal waveform model [57], which includes spin-precession and tidal contributions to the waveform, making it suitable for modeling BNS. To this, we add stationary Gaussian detector noise, with overall noise levels (the power spectral density, PSD) either drawn from a distribution covering an LVK observing run or based on a single PSD (e.g., LVK design sensitivity). When training with a distribution of PSDs, we condition on the PSD, making the network tuned to that observing run, but otherwise able to perform inference with any PSD. Training takes about a week on an H100 GPU. At inference time, we validate and correct results using importance sampling, thus guaranteeing their accuracy (provided a sufficient effective sample size) [27]. We accelerate the importance sampling step using JAX waveform and likelihood implementations [31, 45, 58].

We performed four studies using DINGO-BNS: (a) pre-merger analysis of the first BNS detected, GW170817, and equivalent injections (simulated data sets) at different detector noise levels; (b) pre-merger analysis of varied injections in LVK design sensitivity noise; (c) after-merger analysis of the two detected GW events, GW170817 and GW190425, reproducing published LVK results; and (d) pre-merger analysis of injections in Cosmic Explorer noise (with a minimum frequency of 6 Hz, corresponding to an hour long signal). We use the importance sampling efficiency as a primary performance metric, finding average efficiencies of 45.8%, 41.7%, 17.8%, and 17.1% in experiments, (a), (b), (c), (d), respectively. With these efficiencies, inference for  $10^4$  effective samples typically takes one second on a single H100 GPU (see Supplemental Material). Efficiencies are generally higher for pre-merger inference, as the waveform morphology is most complicated around the merger. In analyses including the merger, we find comparable performance to our past results for black hole mergers (which use a symmetry-enhanced framework [59]), demonstrating the effectiveness of the proposed BNS signal compression. We further observe that XG events are particularly challenging due to their high SNR.

**Discussion.**—Our prior-conditioning approach to data compression works very well for BNS signals, and in the future we would like to extend it to black hole-neutron star systems and low-mass binary black holes. This is nontrivial because such systems can emit GWs in higher angular radiation multipoles (i.e., beyond the  $(l, m) = (2, 2)$  mode that we assume here), which evolve according to integer multiples of (1), and so would require an improved heterodyning algorithm to factor out the chirp. Higher modes are not present in BNS signals since the stars are very nearly equal mass.

Another exciting prospect for SBI is a more realistic

treatment of detector noise. Indeed, since BNS inspirals are long in duration, noise non-stationarities and non-Gaussianities are more likely to manifest within an observation. DINGO-BNS currently assumes stationary Gaussian noise and is supplied with an off-source estimate of the PSD. However, by training on realistic detector noise, our approach can in principle learn to fully characterize the noise jointly with the signal, including any deviations from stationarity and Gaussianity. This approach is akin to on-source PSD and glitch modeling [60], but allows for more general noise and automatically marginalizes over uncertainties. Initial steps in this direction have already been taken for intermediate-mass binary black holes [61]. Improved noise treatments such as those afforded by SBI will become crucial for reducing systematic error as detectors become more sensitive [62].

Finally, although DINGO-BNS is intended to be used for parameter estimation following a trigger by dedicated search pipelines, its speed opens the possibility to run continuously on all data as they are taken. Either the signal-to-noise ratio or Bayesian evidence time series generated by DINGO-BNS could then be used as a detection statistic, forming an end-to-end detection and parameter estimation pipeline. To implement this would require calibrating these statistics to determine false alarm rates, as well as careful comparisons against existing algorithms to establish efficacy.

**Acknowledgments.**—This research has made use of data or software obtained from the Gravitational Wave Open Science Center (gwosc.org), a service of the LIGO Scientific Collaboration, the Virgo Collaboration, and KAGRA. This material is based upon work supported by NSF’s LIGO Laboratory which is a major facility fully funded by the National Science Foundation, as well as the Science and Technology Facilities Council (STFC) of the United Kingdom, the Max-Planck-Society (MPS), and the State of Niedersachsen/Germany for support of the construction of Advanced LIGO and construction and operation of the GEO600 detector. Additional support for Advanced LIGO was provided by the Australian Research Council. Virgo is funded through the European Gravitational Observatory (EGO), by the French Centre National de Recherche Scientifique (CNRS), the Italian Istituto Nazionale di Fisica Nucleare (INFN) and the Dutch Nikhef, with contributions by institutions from Belgium, Germany, Greece, Hungary, Ireland, Japan, Monaco, Poland, Portugal, Spain. KAGRA is supported by Ministry of Education, Culture, Sports, Science and Technology (MEXT), Japan Society for the Promotion of Science (JSPS) in Japan; National Research Foundation (NRF) and Ministry of Science and ICT (MSIT) in Korea; Academia Sinica (AS) and National Science and Technology Council (NSTC) in Taiwan. M.D. thanks the Hector Fellow Academy for support. This work was supported by the German Research Foundation (DFG) through Germany’s Excellence Strategy – EXC- Number 2064/1 –

Project number 390727645). The computational work for this manuscript was carried out on the Atlas cluster at the Max Planck Institute for Intelligent Systems in Tübingen, Germany, and the Lakshmi and Hypatia clusters at the Max Planck Institute for Gravitational Physics in Potsdam, Germany. V.R. is supported by the UK's Science and Technology Facilities Council grant ST/V005618/1.

- 
- [1] B. P. Abbott *et al.* (LIGO Scientific, Virgo), GW170817: Observation of Gravitational Waves from a Binary Neutron Star Inspiral, *Phys. Rev. Lett.* **119**, 161101 (2017), arXiv:1710.05832 [gr-qc].
- [2] B. P. Abbott *et al.* (LIGO Scientific, Virgo, Fermi GBM, INTEGRAL, IceCube, AstroSat Cadmium Zinc Telluride Imager Team, IPN, Insight-Hxmt, ANTARES, Swift, AGILE Team, 1M2H Team, Dark Energy Camera GW-EM, DES, DLT40, GRAWITA, Fermi-LAT, ATCA, ASKAP, Las Cumbres Observatory Group, OzGrav, DWF (Deeper Wider Faster Program), AST3, CAASTRO, VINROUGE, MASTER, J-GEM, GROWTH, JAGWAR, CaltechNRAO, TTU-NRAO, NuSTAR, Pan-STARRS, MAXI Team, TZAC Consortium, KU, Nordic Optical Telescope, ePESSTO, GROND, Texas Tech University, SALT Group, TOROS, BOOTES, MWA, CALET, IKI-GW Follow-up, H.E.S.S., LOFAR, LWA, HAWC, Pierre Auger, ALMA, Euro VLBI Team, Pi of Sky, Chandra Team at McGill University, DFN, ATLAS Telescopes, High Time Resolution Universe Survey, RIMAS, RATIR, SKA South Africa/MeerKAT), Multi-messenger Observations of a Binary Neutron Star Merger, *Astrophys. J. Lett.* **848**, L12 (2017), arXiv:1710.05833 [astro-ph.HE].
- [3] B. P. Abbott *et al.* (LIGO Scientific, Virgo, 1M2H, Dark Energy Camera GW-E, DES, DLT40, Las Cumbres Observatory, VINROUGE, MASTER), A gravitational-wave standard siren measurement of the Hubble constant, *Nature* **551**, 85 (2017), arXiv:1710.05835 [astro-ph.CO].
- [4] B. P. Abbott *et al.* (LIGO Scientific, Virgo, Fermi-GBM, INTEGRAL), Gravitational Waves and Gamma-rays from a Binary Neutron Star Merger: GW170817 and GRB 170817A, *Astrophys. J. Lett.* **848**, L13 (2017), arXiv:1710.05834 [astro-ph.HE].
- [5] B. P. Abbott *et al.* (LIGO Scientific, Virgo), Properties of the binary neutron star merger GW170817, *Phys. Rev.* **X9**, 011001 (2019), arXiv:1805.11579 [gr-qc].
- [6] B. P. Abbott *et al.* (LIGO Scientific, Virgo), GW170817: Measurements of neutron star radii and equation of state, *Phys. Rev. Lett.* **121**, 161101 (2018), arXiv:1805.11581 [gr-qc].
- [7] B. P. Abbott *et al.* (LIGO Scientific, Virgo), Tests of General Relativity with GW170817, *Phys. Rev. Lett.* **123**, 011102 (2019), arXiv:1811.00364 [gr-qc].
- [8] D. A. Coulter *et al.*, Swope Supernova Survey 2017a (SSS17a), the Optical Counterpart to a Gravitational Wave Source, *Science* **358**, 1556 (2017), arXiv:1710.05452 [astro-ph.HE].
- [9] J. Aasi *et al.* (LIGO Scientific), Advanced LIGO, *Class. Quant. Grav.* **32**, 074001 (2015), arXiv:1411.4547 [gr-qc].
- [10] F. Acernese *et al.* (VIRGO), Advanced Virgo: a second-generation interferometric gravitational wave detector, *Class. Quant. Grav.* **32**, 024001 (2015), arXiv:1408.3978 [gr-qc].
- [11] Y. Aso, Y. Michimura, K. Somiya, M. Ando, O. Miyakawa, T. Sekiguchi, D. Tatsumi, and H. Yamamoto (KAGRA), Interferometer design of the KAGRA gravitational wave detector, *Phys. Rev. D* **88**, 043007 (2013), arXiv:1306.6747 [gr-qc].
- [12] J. Veitch, V. Raymond, B. Farr, W. Farr, P. Graff, S. Vitale, *et al.*, Parameter estimation for compact binaries with ground-based gravitational-wave observations using the LALInference software library, *Phys. Rev.* **D91**, 042003 (2015), arXiv:1409.7215 [gr-qc].
- [13] G. Ashton *et al.*, BILBY: A user-friendly Bayesian inference library for gravitational-wave astronomy, *Astrophys. J. Suppl.* **241**, 27 (2019), arXiv:1811.02042 [astro-ph.IM].
- [14] L. S. Finn, Detection, measurement and gravitational radiation, *Phys. Rev. D* **46**, 5236 (1992), arXiv:gr-qc/9209010.
- [15] A. H. Nitz, T. Dal Canton, D. Davis, and S. Reyes, Rapid detection of gravitational waves from compact binary mergers with PyCBC Live, *Phys. Rev. D* **98**, 024050 (2018), arXiv:1805.11174 [gr-qc].
- [16] K. Cannon *et al.*, GstLAL: A software framework for gravitational wave discovery, (2020), arXiv:2010.05082 [astro-ph.IM].
- [17] T. Adams, D. Buskulic, V. Germain, G. M. Guidi, F. Marion, M. Montani, B. Mours, F. Piergiovanni, and G. Wang, Low-latency analysis pipeline for compact binary coalescences in the advanced gravitational wave detector era, *Class. Quant. Grav.* **33**, 175012 (2016), arXiv:1512.02864 [gr-qc].
- [18] Q. Chu *et al.*, SPIIR online coherent pipeline to search for gravitational waves from compact binary coalescences, *Phys. Rev. D* **105**, 024023 (2022), arXiv:2011.06787 [gr-qc].
- [19] S. Sachdev *et al.*, An Early-warning System for Electromagnetic Follow-up of Gravitational-wave Events, *Astrophys. J. Lett.* **905**, L25 (2020), arXiv:2008.04288 [astro-ph.HE].
- [20] A. H. Nitz, M. Schäfer, and T. Dal Canton, Gravitational-wave Merger Forecasting: Scenarios for the Early Detection and Localization of Compact-binary Mergers with Ground-based Observatories, *Astrophys. J. Lett.* **902**, L29 (2020), arXiv:2009.04439 [astro-ph.HE].
- [21] M. Kovalam, M. A. K. Patwary, A. K. Sreekumar, L. Wen, F. H. Panther, and Q. Chu, Early Warnings of Binary Neutron Star Coalescence Using the SPIIR Search, *Astrophys. J. Lett.* **927**, L9 (2022), arXiv:2112.03597 [gr-qc].
- [22] L. P. Singer and L. R. Price, Rapid Bayesian position reconstruction for gravitational-wave transients, *Phys. Rev. D* **93**, 024013 (2016), arXiv:1508.03634 [gr-qc].
- [23] S. Morisaki, R. Smith, L. Tsukada, S. Sachdev, S. Stevenson, C. Talbot, and A. Zimmerman, Rapid localization and inference on compact binary coalescences with the Advanced LIGO-Virgo-KAGRA gravitational-wave detector network, *Phys. Rev. D* **108**, 123040 (2023), arXiv:2307.13380 [gr-qc].
- [24] S. R. Green, C. Simpson, and J. Gair, Gravitational-wave parameter estimation with autoregressive neural network flows, *Phys. Rev. D* **102**, 104057 (2020), arXiv:2002.07656 [astro-ph.IM].
- [25] S. R. Green and J. Gair, Complete parameter inference for GW150914 using deep learning, *Mach. Learn. Sci. Tech.* **2**, 03LT01 (2021), arXiv:2008.03312 [astro-ph.IM].
- [26] M. Dax, S. R. Green, J. Gair, J. H. Macke, A. Buonanno,



- and B. Schölkopf, Real-Time Gravitational Wave Science with Neural Posterior Estimation, *Phys. Rev. Lett.* **127**, 241103 (2021), arXiv:2106.12594 [gr-qc].
- [27] M. Dax, S. R. Green, J. Gair, M. Pürrer, J. Wildberger, J. H. Macke, A. Buonanno, and B. Schölkopf, Neural Importance Sampling for Rapid and Reliable Gravitational-Wave Inference, *Phys. Rev. Lett.* **130**, 171403 (2023), arXiv:2210.05686 [gr-qc].
- [28] S. S. Chaudhary *et al.*, Low-latency gravitational wave alert products and their performance at the time of the fourth LIGO-Virgo-KAGRA observing run, *Proc. Nat. Acad. Sci.* **121**, e2316474121 (2024), arXiv:2308.04545 [astro-ph.HE].
- [29] N. Sridhar, J. Zrake, B. D. Metzger, L. Sironi, and D. Giannios, Shock-powered radio precursors of neutron star mergers from accelerating relativistic binary winds, *Mon. Not. Roy. Astron. Soc.* **501**, 3184 (2021), arXiv:2010.09214 [astro-ph.HE].
- [30] E. R. Most and A. A. Philippov, Electromagnetic precursor flares from the late inspiral of neutron star binaries, *Mon. Not. Roy. Astron. Soc.* **515**, 2710 (2022), arXiv:2205.09643 [astro-ph.HE].
- [31] K. W. K. Wong, M. Isi, and T. D. P. Edwards, Fast Gravitational-wave Parameter Estimation without Compromises, *Astrophys. J.* **958**, 129 (2023), arXiv:2302.05333 [astro-ph.IM].
- [32] D. Reitze *et al.*, Cosmic Explorer: The U.S. Contribution to Gravitational-Wave Astronomy beyond LIGO, *Bull. Am. Astron. Soc.* **51**, 035 (2019), arXiv:1907.04833 [astro-ph.IM].
- [33] M. Punturo *et al.*, The third generation of gravitational wave observatories and their science reach, *Class. Quant. Grav.* **27**, 084007 (2010).
- [34] A. H. Nitz and T. Dal Canton, Pre-merger Localization of Compact-binary Mergers with Third-generation Observatories, *Astrophys. J. Lett.* **917**, L27 (2021), arXiv:2106.15259 [astro-ph.HE].
- [35] E. Cuoco, J. Powell, M. Cavaglià, K. Ackley, M. Berger, C. Chatterjee, M. Coughlin, S. Coughlin, P. Easter, R. Essick, *et al.*, Enhancing gravitational-wave science with machine learning, *Machine Learning: Science and Technology* **2**, 011002 (2020), arXiv:2005.03745 [astro-ph.HE].
- [36] H. Gabbard, C. Messenger, I. S. Heng, F. Tonolini, and R. Murray-Smith, Bayesian parameter estimation using conditional variational autoencoders for gravitational-wave astronomy, *Nature Phys.* **18**, 112 (2022), arXiv:1909.06296 [astro-ph.IM].
- [37] A. Delaunoy, A. Wehenkel, T. Hinderer, S. Nissanke, C. Weniger, A. R. Williamson, and G. Louppe, Lightning-Fast Gravitational Wave Parameter Inference through Neural Amortization, in *Third Workshop on Machine Learning and the Physical Sciences* (2020) arXiv:2010.12931 [astro-ph.IM].
- [38] M. J. Williams, J. Veitch, and C. Messenger, Nested sampling with normalizing flows for gravitational-wave inference, *Phys. Rev. D* **103**, 103006 (2021), arXiv:2102.11056 [gr-qc].
- [39] J. Alvey, U. Bhardwaj, S. Nissanke, and C. Weniger, What to do when things get crowded? Scalable joint analysis of overlapping gravitational wave signals, (2023), arXiv:2308.06318 [gr-qc].
- [40] M. Crisostomi, K. Dey, E. Barausse, and R. Trotta, Neural posterior estimation with guaranteed exact coverage: The ringdown of GW150914, *Phys. Rev. D* **108**, 044029 (2023), arXiv:2305.18528 [gr-qc].
- [41] U. Bhardwaj, J. Alvey, B. K. Miller, S. Nissanke, and C. Weniger, Sequential simulation-based inference for gravitational wave signals, *Phys. Rev. D* **108**, 042004 (2023), arXiv:2304.02035 [gr-qc].
- [42] J. Wildberger, M. Dax, S. Buchholz, S. R. Green, J. H. Macke, and B. Schölkopf, Flow matching for scalable simulation-based inference, *NeurIPS 2023* (2023), arXiv:2305.17161.
- [43] A. Kolmus, J. Janquart, T. Baka, T. van Laarhoven, C. Van Den Broeck, and T. Heskens, Tuning neural posterior estimation for gravitational wave inference, (2024), arXiv:2403.02443 [astro-ph.IM].
- [44] C. Chatterjee and L. Wen, Premerger Sky Localization of Gravitational Waves from Binary Neutron Star Mergers Using Deep Learning, *Astrophys. J.* **959**, 76 (2023), arXiv:2301.03558 [astro-ph.HE].
- [45] T. Wouters, P. T. H. Pang, T. Dietrich, and C. Van Den Broeck, Robust parameter estimation within minutes on gravitational wave signals from binary neutron star inspirals, (2024), arXiv:2404.11397 [astro-ph.IM].
- [46] J. McGinn, A. Mukherjee, J. Irwin, C. Messenger, M. J. Williams, and I. S. Heng, Rapid neutron star equation of state inference with Normalising Flows, (2024), arXiv:2403.17462 [gr-qc].
- [47] Q. Hu and J. Veitch, Rapid Premerger Localization of Binary Neutron Stars in Third-generation Gravitational-wave Detectors, *Astrophys. J. Lett.* **958**, L43 (2023), arXiv:2309.00970 [gr-qc].
- [48] K. Cranmer, J. Brehmer, and G. Louppe, The frontier of simulation-based inference, *Proceedings of the National Academy of Sciences* **117**, 30055 (2020).
- [49] B. P. Abbott *et al.* (LIGO Scientific, Virgo), A guide to LIGO–Virgo detector noise and extraction of transient gravitational-wave signals, *Class. Quant. Grav.* **37**, 055002 (2020), arXiv:1908.11170 [gr-qc].
- [50] N. J. Cornish, Fast Fisher Matrices and Lazy Likelihoods, (2010), arXiv:1007.4820 [gr-qc].
- [51] N. J. Cornish, Heterodyned likelihood for rapid gravitational wave parameter inference, *Phys. Rev. D* **104**, 104054 (2021), arXiv:2109.02728 [gr-qc].
- [52] B. Zackay, L. Dai, and T. Venumadhav, Relative Binning and Fast Likelihood Evaluation for Gravitational Wave Parameter Estimation, (2018), arXiv:1806.08792 [astro-ph.IM].
- [53] S. Vinciguerra, J. Veitch, and I. Mandel, Accelerating gravitational wave parameter estimation with multi-band template interpolation, *Class. Quant. Grav.* **34**, 115006 (2017), arXiv:1703.02062 [gr-qc].
- [54] S. Morisaki, Accelerating parameter estimation of gravitational waves from compact binary coalescence using adaptive frequency resolutions, *Phys. Rev. D* **104**, 044062 (2021), arXiv:2104.07813 [gr-qc].
- [55] L. Blanchet, Gravitational Radiation from Post-Newtonian Sources and Inspiral Compact Binaries, *Living Rev. Rel.* **17**, 2 (2014), arXiv:1310.1528 [gr-qc].
- [56] B. P. Abbott *et al.* (LIGO Scientific, Virgo), Low-latency Gravitational-wave Alerts for Multimessenger Astronomy during the Second Advanced LIGO and Virgo Observing Run, *Astrophys. J.* **875**, 161 (2019), arXiv:1901.03310 [astro-ph.HE].
- [57] T. Dietrich *et al.*, Matter imprints in waveform models for neutron star binaries: Tidal and self-spin effects, *Phys.*

- Rev. D **99**, 024029 (2019), arXiv:1804.02235 [gr-qc].
- [58] T. D. P. Edwards, K. W. K. Wong, K. K. H. Lam, A. Coogan, D. Foreman-Mackey, M. Isi, and A. Zimmerman, ripple: Differentiable and Hardware-Accelerated Waveforms for Gravitational Wave Data Analysis, (2023), arXiv:2302.05329 [astro-ph.IM].
- [59] M. Dax, S. R. Green, J. Gair, M. Deistler, B. Schölkopf, and J. H. Macke, Group equivariant neural posterior estimation, in *International Conference on Learning Representations* (2022) arXiv:2111.13139 [cs.LG].
- [60] N. J. Cornish and T. B. Littenberg, BayesWave: Bayesian Inference for Gravitational Wave Bursts and Instrument Glitches, *Class. Quant. Grav.* **32**, 135012 (2015), arXiv:1410.3835 [gr-qc].
- [61] V. Raymond, S. Al-Shammari, and A. Göttel, Simulation-based Inference for Gravitational-waves from Intermediate-Mass Binary Black Holes in Real Noise, (2024), arXiv:2406.03935 [gr-qc].
- [62] D. Davis *et al.* (LIGO), LIGO detector characterization in the second and third observing runs, *Class. Quant. Grav.* **38**, 135014 (2021), arXiv:2101.11673 [astro-ph.IM].
- [63] G. Papamakarios and I. Murray, Fast  $\epsilon$ -free inference of simulation models with bayesian conditional density estimation, in *Advances in neural information processing systems* (2016) arXiv:1605.06376 [stat.ML].
- [64] J.-M. Lueckmann, P. J. Gonçalves, G. Bassetto, K. Öcal, M. Nonnenmacher, and J. H. Macke, Flexible statistical inference for mechanistic models of neural dynamics, in *Proceedings of the 31st International Conference on Neural Information Processing Systems* (2017) pp. 1289–1299.
- [65] D. Greenberg, M. Nonnenmacher, and J. Macke, Automatic posterior transformation for likelihood-free inference, in *International Conference on Machine Learning* (PMLR, 2019) pp. 2404–2414.
- [66] D. Rezende and S. Mohamed, Variational inference with normalizing flows, in *International Conference on Machine Learning* (2015) pp. 1530–1538, 1505.05770 [stat.ML].
- [67] C. Durkan, A. Bekasov, I. Murray, and G. Papamakarios, Neural spline flows, in *Advances in Neural Information Processing Systems* (2019) pp. 7509–7520, arXiv:1906.04032 [stat.ML].
- [68] M. Deistler, P. J. Goncalves, and J. H. Macke, Truncated proposals for scalable and hassle-free simulation-based inference, *Advances in Neural Information Processing Systems* **35**, 23135 (2022).
- [69] F. Hernandez Vivanco, R. Smith, E. Thrane, P. D. Lasky, C. Talbot, and V. Raymond, Measuring the neutron star equation of state with gravitational waves: The first forty binary neutron star merger observations, *Phys. Rev. D* **100**, 103009 (2019).
- [70] K. He, X. Zhang, S. Ren, and J. Sun, Deep residual learning for image recognition (2015), arXiv:1512.03385 [cs.CV].
- [71] L. Singer, ligo.skymap, <https://lscsoft.docs.ligo.org/ligo.skymap/> (2020).
- [72] B. Abbott *et al.* (LIGO Scientific, Virgo), GW190425: Observation of a Compact Binary Coalescence with Total Mass  $\sim 3.4M_{\odot}$ , *Astrophys. J. Lett.* **892**, L3 (2020), arXiv:2001.01761 [astro-ph.HE].
- [73] J. Wildberger, M. Dax, S. R. Green, J. Gair, M. Pürrer, J. H. Macke, A. Buonanno, and B. Schölkopf, Adapting to noise distribution shifts in flow-based gravitational-wave inference, *Phys. Rev. D* **107**, 084046 (2023), arXiv:2211.08801 [gr-qc].



## Supplemental Material

### MACHINE LEARNING FRAMEWORK

The Bayesian posterior  $p(\theta|d) = p(d|\theta)p(\theta)/p(d)$  is defined in terms of a prior  $p(\theta)$  and a likelihood  $p(d|\theta)$ . For GW inference, the likelihood is constructed by combining models for waveforms and detector noise. The Bayesian evidence  $p(d)$  corresponds to the normalization of the posterior, and it can be used for model comparison.

Our framework is based on neural posterior estimation (NPE) [63–65], which trains a density estimation neural network  $q(\theta|d)$  to estimate  $p(\theta|d)$ . We parameterize  $q(\theta|d)$  with a conditional normalizing flow [66, 67]. Training minimizes the loss  $L = -\log q(\theta|d)$  across a dataset  $(\theta_i, d_i)$  of parameters  $\theta_i \sim p(\theta)$  paired with corresponding likelihood simulations  $d_i \sim p(d|\theta_i)$ . After training,  $q(\theta|d)$  serves as a surrogate for  $p(\theta|d)$ , and inference for any observed data  $d_o$  can be performed by sampling  $\theta \sim q(\theta|d_o)$ . DINGO [26, 27] uses a group-equivariant formulation of NPE (GNPE [26, 59]), which simplifies GW data based on physical symmetries at the cost of longer inference times. We do not use GNPE for DINGO-BNS to achieve faster inference, and compensate for the more difficult inference task with larger neural networks, bigger training data sets, and longer training times (see experimental details).

At inference, we correct for potential inaccuracies of  $q(\theta|d)$  with importance sampling [27], by assigning a weight  $w_i = p(d|\theta_i)p(\theta_i)/q(\theta_i|d)$  to each sample  $\theta_i \sim q(\theta_i|d)$ . A set of  $n$  weighted samples  $(w_i, \theta_i)$  corresponds to  $n_{\text{eff}} = (\sum_i w_i)^2 / (\sum_i w_i^2)$  effective samples from the posterior  $p(\theta|d)$ . This reweighting enables asymptotically exact results, and the sample efficiency  $\epsilon = n_{\text{eff}}/n$  serves as a performance metric. The normalization of the weights further provides an unbiased estimate of the Bayesian evidence  $p(d) = (\sum_i w_i) / n$ .

Below, we describe in more detail the technical innovations of DINGO-BNS that enable scaling of this framework to BNS signals.

#### Prior conditioning

An NPE model  $q(\theta|d)$  estimates the posterior  $p(\theta|d)$  for a fixed prior  $p(\theta)$ . Choosing a broad prior enhances the general applicability of the NPE model, but it also implies worse tuning to specific events (for which smaller priors may be sufficient). This is a general trade-off in NPE, but it is particularly dramatic for BNS inference, where the chirp mass is extremely well constrained by the data but varies strongly between different events. We resolve this trade-off with a new technique called prior conditioning. The key idea is to train an NPE model with *multiple different* priors simultaneously. Training a prior-conditioned model requires hierarchical sampling of

$\theta$

$$\theta \sim p_\rho(\theta), \quad \rho \sim \hat{p}(\rho), \quad (2)$$

where  $p_\rho(\theta)$  is a prior family parameterized by  $\rho$  and  $\hat{p}(\rho)$  is a corresponding hyperprior. We additionally condition the NPE model  $q(\theta|d, \rho)$  on  $\rho$ . This model can then perform inference for any desired prior  $p_\rho(\theta)$ , by simply providing the corresponding  $\rho$ . This effectively amortizes the training cost over different choices of the prior.

We apply prior conditioning for the chirp mass  $\mathcal{M}$ , using a set of priors  $p_{\tilde{\mathcal{M}}}(\mathcal{M}) = U_{m_1, m_2}(\mathcal{M} - \Delta\mathcal{M}, \mathcal{M} + \Delta\mathcal{M})$ . Here,  $U_{m_1, m_2}(\mathcal{M}_{\min}, \mathcal{M}_{\max})$  denotes a distribution over  $\mathcal{M}$  with support  $[\mathcal{M}_{\min}, \mathcal{M}_{\max}]$ , within which component masses  $m_1, m_2$  are uniformly distributed. We use fixed  $\Delta\mathcal{M} = 0.005 M_\odot$  and choose a hyperprior  $\hat{p}(\tilde{\mathcal{M}})$  covering the expected range of  $\mathcal{M}$  for LVK detections of BNS (see Tab. II). As  $\Delta\mathcal{M}$  is small,  $\tilde{\mathcal{M}}$  is a good approximation for any  $\mathcal{M}$  within the restricted prior  $p_{\tilde{\mathcal{M}}}(\mathcal{M})$  and we can thus use  $\tilde{\mathcal{M}}$  for heterodyning. The resulting model  $q(\theta|d_{\tilde{\mathcal{M}}}, \tilde{\mathcal{M}})$  can then perform inference with event-optimized heterodyning and prior (via choice of appropriate  $\tilde{\mathcal{M}}$ ), but is nevertheless applicable to the entire range of the hyperprior.

Inference results are independent of  $\tilde{\mathcal{M}}$  as long as the posterior  $p(\mathcal{M}|d)$  is fully covered by  $[\tilde{\mathcal{M}} - \Delta\mathcal{M}, \tilde{\mathcal{M}} + \Delta\mathcal{M}]$ . For BNS,  $p(\mathcal{M}|d)$  is typically tightly constrained and we can use a coarse estimate of  $\mathcal{M}$  for  $\tilde{\mathcal{M}}$ . This can either be taken from a GW search pipeline or rapidly computed from  $q(\theta|d_{\tilde{\mathcal{M}}}, \tilde{\mathcal{M}})$  itself by sweeping the hyperprior (see below). Note that for shorter GW signals from black hole mergers,  $p(\mathcal{M}|d)$  is generally less well constrained. Transfer of prior conditioning would thus require larger (and potentially flexible) values of  $\Delta\mathcal{M}$ . Alternatively, the prior range can be extended at inference time by iterative Gibbs sampling of  $\mathcal{M}$  and  $\tilde{\mathcal{M}}$ , similar to the GNPE algorithm [26, 59].

Prior conditioning is a general SBI technique that enables choice of prior at inference time. This can also be achieved with sequential NPE [63–65, 68]. However, in contrast to prior conditioning, these techniques require simulations and retraining for each observation, resulting in more expensive and slower inference. We here use prior conditioning with priors of fixed width for the chirp mass, and optional additional conditioning on fixed values for other parameters (corresponding to Dirac delta priors). Extension to more complicated priors and hyperpriors is straightforward.

#### Independent estimation of chirp mass and merger times

Running DINGO-BNS requires an initial estimate of the chirp mass  $\mathcal{M}$  (to determine  $\tilde{\mathcal{M}}$  for the network) and the merger time  $t_c$  (to trigger the analysis). Matched

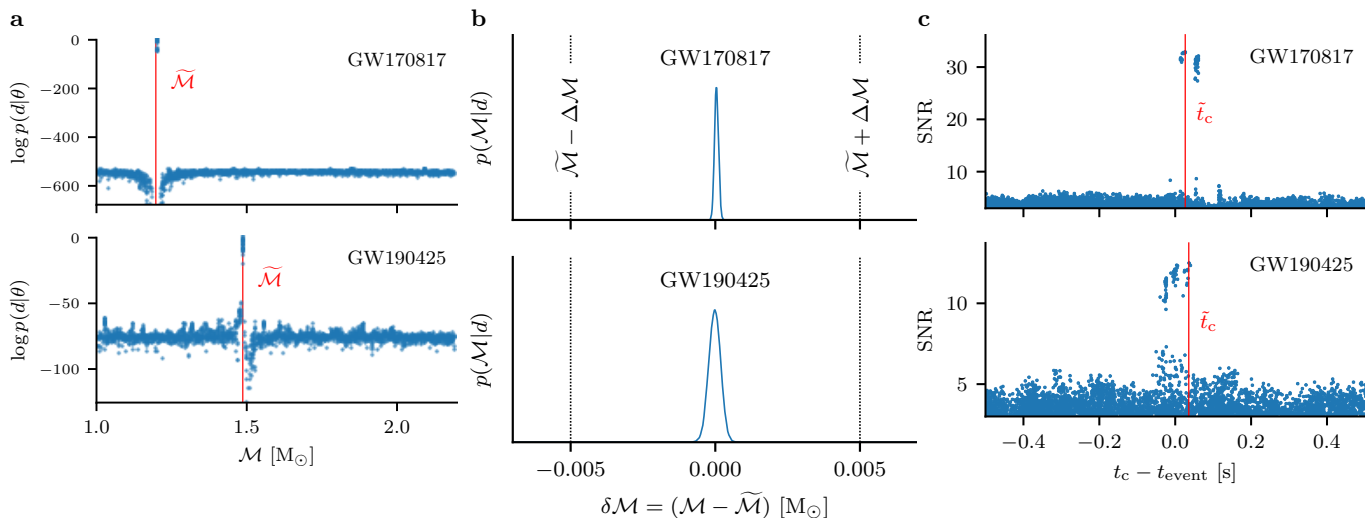


Figure 4. (a) Log likelihoods generated from a scan over different values of  $\tilde{\mathcal{M}}$  with a DINGO-BNS network. The final  $\tilde{\mathcal{M}}$  is chosen as the maximum likelihood  $\mathcal{M}$  (red line;  $\tilde{\mathcal{M}} = 1.1975$  M $_{\odot}$  for GW170817,  $\tilde{\mathcal{M}} = 1.4868$  M $_{\odot}$  for GW190425). (b) Posterior marginal  $p(\mathcal{M}|d)$ . The prior (dashed lines) determined by the scan from (a) fully covers the marginal. (c) A combined scan over  $\mathcal{M}$  and  $t_c$  successfully identifies GW170817 (with  $\hat{t}_c = 1187008882.43$ ) and GW190425 (with  $\hat{t}_c = 1240215503.04$ ).

$\Delta f_i$ [Hz]	LVK		CE
	$\hat{f}_i$ [Hz]	$\hat{f}_i$ [Hz]	
1/8192			5
1/4096			5
1/2048			5
1/1024			7
1/512			10
1/256			13
1/128	19		18
1/64	25		24
1/32	34		32
1/16	44		42
1/8	57		54
1/4	72		68
1/2	89		84
1	420		364
2			765

Table I. Multi-banded frequency domain partitions for LVK ( $f_{\min} = 19.4$  Hz, compression factor  $\sim 60$ ) and CE ( $f_{\min} = 5$  Hz, compression factor  $\sim 650$ ) experiments. We use a smaller chirp mass prior for the CE experiments (Tab. II), which allows a slightly coarser resolution (corresponding to lower  $\hat{f}_i$ ). The first two bands for CE are skipped entirely, which is a consequence of the reduced signal variation with heterodyning.

filter searches can identify the presence of a compact binary signal and its chirp mass and merger time in low-latency [14–18]. Specialized “early warning” searches designed to produce output before the coalescence can further provide a rough indication of sky position and distance [19–21]. When available, output of such pipelines can be used to trigger a DINGO analysis and provide the estimates for  $\mathcal{M}$  and  $t_c$ .

We here describe an alternative independent approach

of obtaining these parameters, using only the trained DINGO-BNS model. We compute  $\tilde{\mathcal{M}}$  by sweeping the entire hyperprior  $\hat{p}(\tilde{\mathcal{M}}) = U_{m_1, m_2}(\tilde{\mathcal{M}}_{\min}, \tilde{\mathcal{M}}_{\max})$ . Specifically, we run DINGO-BNS with a set of prior centers

$$\tilde{\mathcal{M}}_i = \tilde{\mathcal{M}}_{\min} + i \cdot \Delta\mathcal{M}, \quad i \in [0, (\tilde{\mathcal{M}}_{\max} - \tilde{\mathcal{M}}_{\min}) / \Delta\mathcal{M}]. \quad (3)$$

The inference models in this study are trained with hyperprior ranges of up to  $[1.0, 2.2]$  M $_{\odot}$ . For  $\Delta\mathcal{M} = 0.005$  M $_{\odot}$ , we can thus cover the entire global chirp mass range using 241 (overlapping) local priors. We run DINGO-BNS for all local priors  $\tilde{\mathcal{M}}_i$  in parallel, with 10 samples per  $\tilde{\mathcal{M}}_i$ . This requires DINGO-BNS inference of only a few thousand samples, which takes less than one second. We use the chirp mass  $\mathcal{M}$  of the maximum likelihood sample as the prior center  $\tilde{\mathcal{M}}$  for the analysis (Fig. 4a). Note that the exact choice of  $\tilde{\mathcal{M}}$  does not matter, as long as the inferred posterior is fully covered by  $[\tilde{\mathcal{M}} - \Delta\mathcal{M}, \tilde{\mathcal{M}} + \Delta\mathcal{M}]$  (Fig. 4b).

The merger time  $t_c$  can be inferred by continuously running this  $\tilde{\mathcal{M}}$  scan on the input data stream, sliding the  $t_c$  prior in real time over the incoming data. With inference times of one second and a prior  $p(t_c) = U(-300 \text{ ms}, +300 \text{ ms})$  for the merger time, continuous analysis could be achieved on just two parallel computational nodes, constantly running on the input data stream. Event candidates can then be identified by analyzing the SNR, triggering upon exceeding some defined threshold (Fig. 4c). This scan could be performed at an arbitrary (but fixed) time prior to the merger.

This scan successfully estimates  $\mathcal{M}$  and  $t_c$  for both real BNS events (Fig 4). However, we have not tested this at a large scale on detector noise to compute false alarm rates, as DINGO-BNS is primarily intended for

parameter estimation. Existing search and early warning pipelines are likely more robust for event identification, in particular in the presence of non-stationary detector noise.

### Frequency multibanding

While the native resolution of a frequency series is generally determined by the duration  $T$  of the corresponding time series ( $\Delta f = 1/T$ ), we can average neighboring frequency bins whenever the signal in these is constant. This enables data compression with only negligible loss of information. We here employ frequency multibanding, which divides the frequency range  $[f_{\min}, f_{\max}]$  into  $N$  adjacent bands of decreasing resolution. Frequency band  $i$  covers the range  $[f_i, f_{i+1})$  with  $\Delta f_i = 2^i \Delta f_0$ , where  $\hat{f}_0 = f_{\min}$ ,  $\hat{f}_N = f_{\max}$  and  $\Delta f_0$  is the native resolution of the frequency series. To achieve optimal compression, we empirically choose the smallest possible nodes  $\hat{f}_i$  that still fully resolve the relevant GW signals. Specifically, we simulate a set of  $10^3$  heterodyned GW signals during training and demand that every period of these signals is covered by at least 32 ‘‘decimation windows’’ (see below) in the resulting multibanded frequency domain. This optimized resolution achieves compression factors between 60 and 650 (Tab. I).

We can save memory and computation by directly evaluating the GW data and signal in the multibanded domain rather than the base frequency domain. The whitened strain data is given by

$$d_j^w = h_j^w(\theta) + n_j^w = \frac{h_j(\theta) + n_j}{\sqrt{S_j}}. \quad (4)$$

Here,  $h_j$  and  $n_j$  are the waveform and noise respectively in the  $j$ th frequency bin. By construction, the whitened noise has a constant variance,

$$n_j^w \sim \mathcal{N}(0, \sigma_n), \quad (5)$$

where  $\sigma_n = \sqrt{\frac{w}{4\Delta f_0}}$  and  $w$  is the Tukey window factor. In each band,  $i$ , we decompose the signal into ‘‘decimation windows’’,  $[j_i^-, j_i^+)$ , each containing  $N_i$  bins. We can then average the whitened data in the decimation window centered on  $j_i$

$$\begin{aligned} \overline{d_{j_i}^w} &= \frac{1}{N_i} \sum_{j=j_i^-}^{j_i^+} (h_j^w + n_j^w) = \overline{h_{j_i}^w} + \overline{n_{j_i}^w}, \\ j_i^\pm &= j_i \pm \frac{N_i - 1}{2}. \end{aligned} \quad (6)$$

Note here we are abusing notation by indexing  $\overline{d^w}$ ,  $\overline{h^w}$  and  $\overline{n^w}$  with the bin at the center of the decimation window,  $j_i$ .

Since  $\overline{n_{j_i}^w}$  is an average of  $N_i$  Gaussian random variables,  $\{\overline{n_j^w} | j \in [j_i^-, j_i^+]\}$ , it follows that  $\overline{n_{j_i}^w}$  is distributed as a Gaussian but with mean zero and variance

$$(\overline{\sigma_i^w})^2 = \frac{1}{N_i^2} \sum_j^{N_i} \sigma_n^2 = \frac{w}{4\Delta f_i}. \quad (7)$$

We have used the relation  $\Delta f_i = \Delta f_0 N_i$  in the last equality. Finally, the decimated whitened signal is given by

$$\overline{h_{j_i}^w} = \frac{1}{N_i} \sum_{j=j_i^-}^{j_i^+} \frac{h_j}{\sqrt{S_j}} \approx h_{j_i} \sum_{j=j_i^-}^{j_i^+} \frac{1}{\sqrt{S_j}}. \quad (8)$$

The approximate equality is because in each decimation window, the waveform is approximately constant. This follows as we have chosen at least 32 decimation windows per period of the waveform.

We can now compute the likelihood using the standard Whittle likelihood used in GW astronomy [49] except using the decimated whitened data and signal. Explicitly, this is

$$\log p(d|\theta) \approx -\frac{1}{2} \sum_{i=0}^N (\overline{\sigma_i^w})^{-2} \sum_{j_i} |\overline{d_{j_i}^w} - \overline{h_{j_i}^w}|^2, \quad (9)$$

where the first sum is over the bands and the second is over the decimation windows in each band. We here use this approximate multibanded likelihood also for importance sampling. We found these approximations to have a negligible impact in practice. However, if desired, DINGO-BNS can also use the full (more expensive) likelihood for importance sampling, and potentially accelerate this using the reduced order quadrature technique from [23].

### Frequency masking

Our framework operates in frequency domain, but observed GW data is originally represented as a time series. Time series data is converted to frequency domain by windowing and subsequent Fourier transformation. The finite duration of the Fourier-transformed time segment  $[t_{\min}, t_{\max}]$  implies, that not all frequencies are accurately captured by the resulting frequency series. In our analysis, we thus need to omit all frequencies present in the signal for  $t < t_{\min}$  and  $t > t_{\max}$ . This avoids mismatches between data and theoretical frequency domain models (which assume infinite duration). As the frequency evolution of the inspiral is tightly constrained by the chirp mass  $\mathcal{M}$ , we can compute boundaries  $f_{\min}(t_{\min}, \mathcal{M})$  and  $f_{\max}(t_{\max}, \mathcal{M})$ , such that signals are not corrupted by finite-duration effects within  $[f_{\min}, f_{\max}]$ , and are negligibly small outside of that range (Fig. 5).

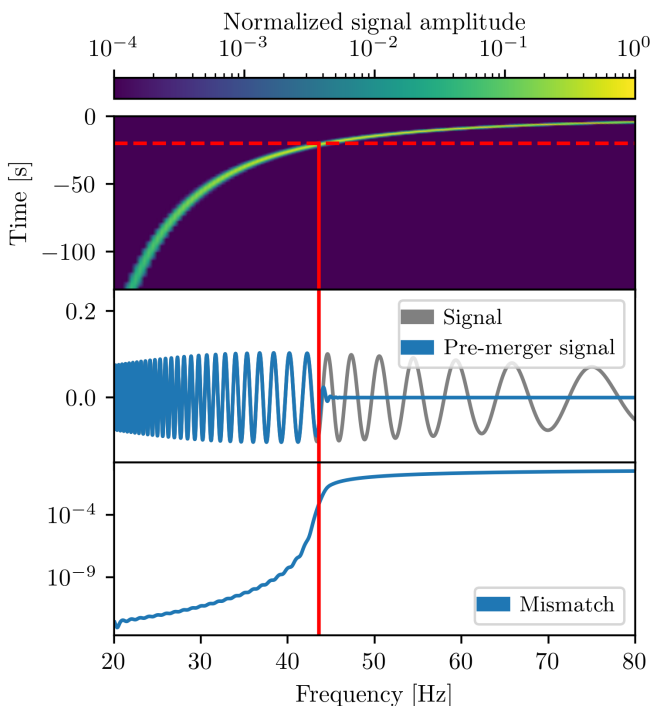


Figure 5. Time-domain truncation of BNS signals at time  $t_{\max}$  (red dashed line) before the merger can be approximated by truncation at a corresponding maximum frequency (red solid line) in frequency domain. Below frequency  $f_{\max}(t, \mathcal{M})$ , the truncated signal (blue in center panel) matches the original signal (gray). Above  $f_{\max}(t, \mathcal{M})$ , the amplitude of the truncated signal quickly approaches zero. We determine  $f_{\max}(t, \mathcal{M})$  empirically, by allowing mismatches between truncated and original signals of at most  $10^{-3}$  (lower panel). Analogously, truncation for  $t < t_{\min}$  can be achieved by imposing a minimum frequency cutoff  $f_{\min}(t, \mathcal{M})$ .

We approximate the lower bound  $f_{\min}(t_{\min}, \mathcal{M})$  using the leading order in the post-Newtonian relationship between time and frequency,

$$f_{\text{0PN}}(t, \mathcal{M}) = \frac{1}{8\pi} \left( \frac{-t}{5} \right)^{-3/8} \mathcal{M}^{-5/8}. \quad (10)$$

For a Dingo network designed for fixed data duration  $T$ , we set  $f_{\min}(T, \mathcal{M}) = f_{\text{0PN}}(-T, \mathcal{M}) + f_{\text{buffer}}$  (we use  $f_{\text{buffer}} = 1$  Hz for LVK and  $f_{\text{buffer}} = 0.5$  Hz for XG setups).

For the upper bound, we found that  $f_{\text{0PN}}(t, \mathcal{M})$  is not sufficiently accurate. Instead, we determine  $f_{\max}(t, \mathcal{M})$  empirically by simulating a set of signals (with parameters  $\theta \sim p(\theta)$ ), and computing mismatches between signals with and without truncation at  $t > t_{\max}$ . For a given set of simulations, we choose  $f_{\max}(t, \mathcal{M})$  as the highest frequency for which all mismatches are at most  $10^{-3}$ . To avoid additional computation at inference time, we cache the results in a lookup table for  $f_{\max}(t, \mathcal{M})$ .

Both bounds depend on the chirp mass  $\mathcal{M}$ , and the upper bound additionally depends on the pre-merger time. To enable inference for arbitrary configurations, we train

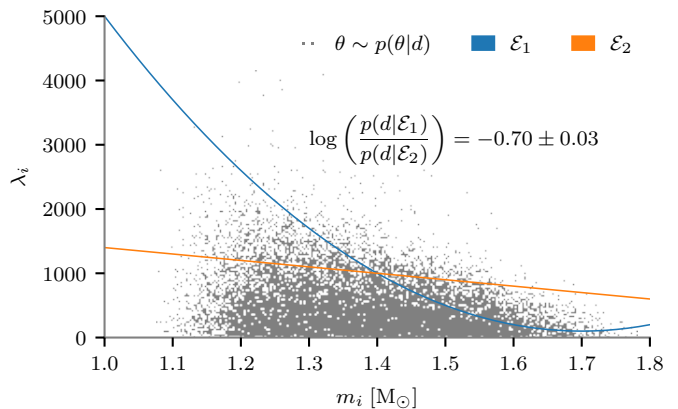


Figure 6. Neutron-star EOS imply a functional relation  $\lambda_i = \lambda_i(m_i)$  between tidal parameters  $\lambda_i$  and the component masses. The likelihood  $p(d|\mathcal{E})$  for an EOS  $\mathcal{E}$  given the GW data  $d$  requires integrating the posterior  $p(\theta|d)$  along the corresponding hyperplane. No posterior will be exactly on that hyperplane, hence the standard Bayesian inference techniques are not directly applicable [69]. DINGO-BNS provides various possibilities to directly compute this quantity due to its flexibility with respect to conditioning and marginalization.

a single dingo network with dynamic frequency masking. During training, we compute  $f_{\min}(T, \widetilde{\mathcal{M}})$  with the center  $\widetilde{\mathcal{M}}$  of the local chirp mass prior. The upper frequency bound  $f_{\max}$  is sampled randomly (uniform in frequency bins of the multibanded frequency domain) to allow for arbitrary pre-merger times. Data outside of  $[f_{\min}, f_{\max}]$  is zero-masked.

### Equation-of-state likelihood

A nuclear equation of state (EOS) implies a functional relationship between neutron star masses  $m_i$  and tidal deformabilities  $\lambda_i$ . The likelihood  $p(d|\mathcal{E})$  for a given EOS  $\mathcal{E}$  and data  $d$  can be computed by integrating the GW likelihood along the hyperplane defined by the EOS constraint  $\lambda_i = \lambda_i^{\mathcal{E}}(m_i)$ ,

$$\begin{aligned} p(d|\mathcal{E}) &= \int p(d|\theta) p(\theta) \delta(\lambda_i = -\lambda_i^{\mathcal{E}}(m_i)) d\theta \\ &= \int p(d|m_1, m_2, \lambda_1^{\mathcal{E}}(m_1), \lambda_2^{\mathcal{E}}(m_2)) dm_1 dm_2. \end{aligned} \quad (11)$$

Here,  $p(d|m_1, m_2, \lambda_1, \lambda_2)$  is the Bayesian evidence of  $d$  for fixed  $m_1, m_2, \lambda_1, \lambda_2$ . With traditional methods (e.g., nested sampling), it is extremely expensive to estimate this quantity, such that  $p(d|\mathcal{E})$  can not be computed by direct integration. DINGO-BNS, however, provides rapid estimates of the Bayesian evidence  $p(d)$ . With a DINGO-BNS network conditioned on  $(m_1, m_2, \lambda_1, \lambda_2)$ , we can thus estimate  $p(d|m_1, m_2, \lambda_1, \lambda_2)$  within less than a second, making the two dimensional integration in Eq. (11) computationally possible (Fig. 6). Alternatively, one can

	LVK	CE
$\mathcal{M}$ [ $M_{\odot}$ ]	[1.0, 2.2]	[1.15, 1.25]
$m_1$	[1.0, 3.2]	[0.95, 2.4]
$m_2$	[1.0, 2.0]	[0.95, 2.4]
$a_{1,2}$	[0, 0.05]	[0, 0.05]
$\lambda_1$	[0, 5000]	[0, 5000]
$\lambda_2$	[0, 10000]	[0, 10000]
$d_L$ [Mpc]	[10, 100]	[20, 50] / [1000, 2000]
$t_c$ [s]	[-0.1, 0.1] / [-0.03, 0.03]	[-1, 1] / [-0.03, 0.03]

Table II. Training priors for chirp mass  $\mathcal{M}$ , component masses  $m_{1,2}$ , spin magnitudes  $a_{1,2}$ , tidal deformabilities  $\lambda_{1,2}$ , luminosity distance  $d_L$  and merger time  $t_c$ . All priors are uniform, except for chirp mass, which is sampled uniform in component masses. At inference,  $d_L$  can be reweighted to the standard prior (uniform in comoving volume). For  $t_c$  we use a broader prior for pre-merger inference than for full inference (separated by “/” symbol) to account for higher uncertainties. LVK priors are chosen to cover expected LVK BNS detections. CE priors for  $\mathcal{M}$  and  $d_L$  are reduced compared to LVK to decrease the computational cost of training. Priors for parameters not displayed here are standard.

estimate a marginalized posterior  $p(m_1, m_2, \lambda_1, \lambda_2 | d)$  with DINGO-BNS, which provides a direct (unnormalized) estimate for  $p(d | m_1, m_2, \lambda_1, \lambda_2)$ . This method allows for even faster integration of Eq. (11), but does not directly allow for validation with importance sampling. Finally, one could also condition DINGO-BNS directly on EOS parameterizations. These methods are enabled by the flexibility of SBI to condition on or marginalize over arbitrary parameters can

## EXPERIMENTAL DETAILS

For our experiments, we train DINGO-BNS networks using the hyperparameters and neural architecture [67, 70] from Ref. [26], with a slightly larger embedding network. For the LVK experiments, we use a dataset with  $3 \cdot 10^7$  training samples and train for 200 epochs, for CE we use  $6 \cdot 10^7$  training samples and train for 100 epochs. We use three detectors for LVK (LIGO-Hanford, LIGO-Livingston, and Virgo) and two detectors for CE (primary detector at location of LIGO-Hanford, secondary detector at location of LIGO-Livingston). The networks are trained with the priors displayed in Tab. II.

In the first experiment, we evaluate DINGO-BNS models on 200 simulated GW datasets, generated using a fixed GW signal with GW170817-like parameters and simulated LVK detector noise. We use noise PSDs from the second (O2) and third (O3) LVK observing runs as well as LVK design sensitivity. For each noise level, we train one pre-merger network ( $f \in [23, 200]$  Hz) and one network for inference with the full signal, including the merger ( $f \in [23, 1024]$ ). The latter network is only used for inference after the merger, as we found that the separation

into two networks improved the performance. The pre-merger network is trained with frequency masking with the masking bound  $f_{\max}$  sampled in range [28, 200] Hz, enabling inference up to 60 seconds before the merger.

In the second experiment, we analyze 1000 simulated GW datasets, with GW signal parameters randomly sampled from the prior (Tab. II;  $\mathcal{M}$  prior reduced to range [1.0, 1.5]  $M_{\odot}$  and  $d_L$  prior reweighted to a uniform distribution in comoving volume) and with design sensitivity noise PSDs. We again train one pre-merger network ( $f \in [19.4, 200]$  Hz) and one network for full inference ( $f \in [19.4, 1024]$  Hz). The pre-merger network is trained with frequency masking with the masking bound  $f_{\max}$  sampled in range [25, 200] Hz, enabling inference up to 60 seconds before the merger for  $\mathcal{M} \leq 1.5 M_{\odot}$ . Both networks are additionally trained with lower frequency masking, with  $f_{\min}(\mathcal{M})$  determined as explained above, ensuring an optimal frequency range for any chirp mass. For each DINGO-BNS result, we generate a skymap using a kernel density estimator implemented by `ligo.skymap` [71]. For the sky localization comparison between DINGO-BNS and Bayestar, we run Bayestar based on the GW signal template generated with the maximum likelihood parameters from the DINGO-BNS analysis. We note that Bayestar is designed as a low-latency pipeline and typically run with (coarser) parameter estimates from search templates. Therefore, the reported Bayestar runs may deviate slightly from the realistic LVK setup. However, our results are consistent with [23], who also found a  $\sim 30\%$  precision improvement over Bayestar localization (using LVK search triggers). Both, DINGO-BNS and Ref. [23], perform full Bayesian BNS inference and should therefore have identical localization improvements over Bayestar (assuming ideal accuracy, which for DINGO-BNS is validated with consistently high importance sampling efficiency). Differences to the localization comparison in Ref [23] are thus primarily attributed to different configurations for Bayestar and slightly different injection priors. Additional results for the localization comparison are shown in Fig. 7.

In the third experiment, we reproduce the public LVK results for GW170817 [1, 5] and GW190425 [72] with DINGO-BNS. We use the same prior and data settings as the LVK, but we do not marginalize over calibration uncertainty. We find good sample efficiencies for both events (10.8% for GW170817 and 51.3% for GW190425) and good agreement with the LVK results (Fig. 8).

In the fourth experiment, we analyze simulated CE data using the anticipated noise PSDs for the primary and secondary detectors. We train a DINGO-BNS network for pre-merger inference with  $f \in [6, 11]$  Hz, with the upper frequency masking bound  $f_{\max}$  sampled in range [7, 11] Hz. This supports a signal length of 4096 seconds, with pre-merger inference between 45 and 15 minutes prior to the merger. We inject signals with GW170817-like parameters for distance, masses and inclination, to

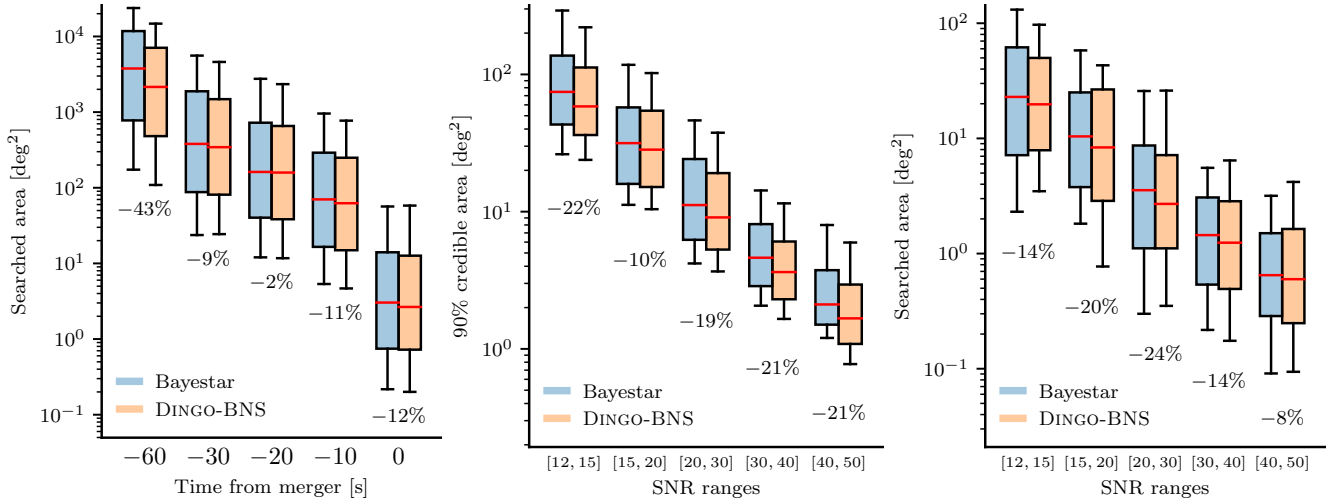


Figure 7. Localization comparison between Bayestar and Dingo-BNS, in terms of the 90% credible area and the searched area. The comparisons according to SNR are based only on results after the merger.

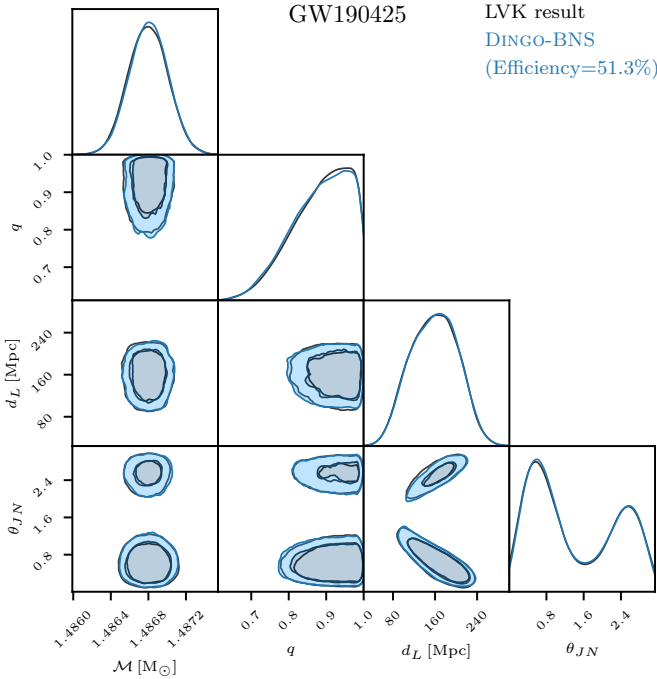


Figure 8. Inference results for GW190425. DINGO-BNS shows good agreement with the public LVK result.

investigate how well GW170817-like event can be localized in the CE detector. We also train a network on the full frequency range [6, 1024] Hz for inference with the full signal, with a reduced distance prior to control the SNR (Tab. II).

**Sample efficiencies**

We report sample efficiencies for all injections studies in Fig. 9. Importance-sampled DINGO-BNS results are accurate even with low efficiency, provided that a sufficient *absolute* number of effective samples can be generated. The efficiency nevertheless is a valuable diagnostic to assess the performance of the trained inference networks.

In LVK experiments, we find consistently high efficiencies, comparable to or higher than those reported for binary black holes [27]. As a general trend, we observe that higher noise levels (Fig. 9a) and earlier pre-merger times (Fig. 9b) lead to higher efficiencies. This is because low SNR events generally have broader posteriors, which are simpler to model for DINGO-BNS density estimators. Furthermore, the GW signal morphology is most complicated around the merger, making pre-merger inference a much simpler than inference based on the full signal.

For CE injections with GW170817-like parameters (Fig. 9c), DINGO-BNS achieves extremely high efficiency for early pre-merger analyses but the performance decreases substantially for later analysis times. This effect can again be attributed to the increase in SNR, which is of order  $\mathcal{O}(10^3)$  15 minutes before the merger. Improving DINGO-BNS for such high SNR events will likely require improved density estimators [42] that can better deal with tighter posteriors. When limiting the SNR by increasing the distance prior (Tab. II), we find good sample efficiencies for a full CE analysis, that uses the full 4096 second long signal, including the merger (Fig. 9c).

**Inference times**

The computational cost of inference with DINGO-BNS is dominated by (1) neural network forward passes to sam-



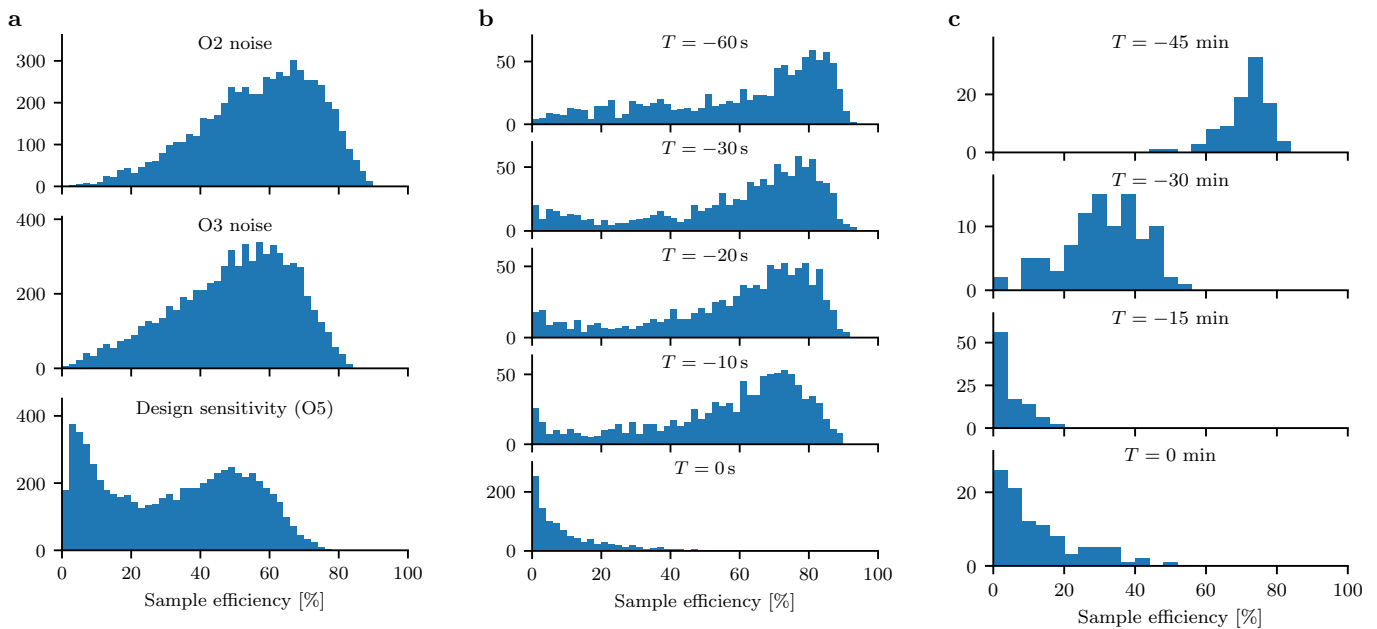


Figure 9. Sample efficiencies for the injection studies. (a) GW170817-like injections using different detector noise levels. (b) Injections using LVK design sensitivity PSDs. (c) Injections using CE PSDs.

ple from the approximate posterior  $\theta \sim q(\theta|d_{\tilde{\mathcal{M}}}, \tilde{\mathcal{M}})$  and by (2) likelihood evaluations  $p(\theta|d)$  used for importance sampling. For 50,000 samples on an H100 GPU, (1) takes  $\sim 0.370$  seconds and (2) takes  $\sim 0.190$  seconds, resulting in an inference time of less than 0.6 seconds. The speed of the likelihood evaluations is enabled by using JAX waveform and likelihood implementations [31, 45, 58], combined with the heterodyning and multibanding step that we also use to compress the data for the DINGO-BNS network. We can jit the likelihood ahead of time since we evaluate a fixed number of waveforms at a fixed number of frequency bins. Thus we leave the jitting time (18 seconds) out of the timing estimate for importance sampling. This is in contrast to previous JAX-based GW works [31, 45] which use a fiducial waveform (determined at inference time via likelihood maximization) to perform heterodyning. Likelihood evaluations can also be done without JAX, which takes less than 10 seconds on a single node with 64 CPUs for 50,000 samples. For the vast majority of DINGO-BNS analyses in this study, the sample efficiency is sufficiently high such that 50,000 samples correspond to several thousands of effective samples after

importance sampling, enabling full importance sampling inference in less than a second. Note that these times only include neural network forward passes and likelihood evaluations. Integration into LVK pipelines will add some additional latency.

### PSD tuning

Most of the networks used in this study are trained with only a single PSD per detector. However, DINGO-BNS can be trained with an entire distribution of PSDs, enabling instant tuning to drifting detector noise [26]. This makes the inference task more complicated, and therefore leads to slightly reduced performance. For example, when repeating the first injection experiment (Fig. 9a) with a DINGO-BNS network trained with a distribution covering the entire second LVK observing run, the median efficiency is reduced from 59% to 24%. Such networks can in principle also be trained before the start of an observing run, by training with a synthetic dataset designed to reflect the expected noise PSDs [73].